
The Adjustment of the Wind Field to Small Scale Topography In a Numerical Weather Prediction Model

Hubert Allard¹ and Jacques Derome

Department of Meteorology, McGill University

[Manuscript received 26 August 1974; in revised form 21 October 1974]

ABSTRACT

Numerical experiments are performed to test one reasonably economical method of producing regional forecasts. Starting with initial conditions interpolated from a 20 hour coarse grid Northern Hemisphere forecast, a fine mesh model is integrated for a further period of 4 hours over a limited area. The fine mesh is located over the north-eastern part of North America and its resolution is sufficient to re-

produce topographic features such as the St. Lawrence and Richelieu Valleys. The resulting forecast at hour 24 is then compared with the coarse mesh prediction for the same time. The comparison reveals how the horizontal and vertical components of the wind are affected by the small scale topography. In particular, the channelling effect of the main valleys is demonstrated.

1 Introduction

Most numerical weather prediction models in operational use take into account the large scale features of the main mountain barriers but lack the spatial resolution necessary to reproduce explicitly the characteristics of the ground on a subsynoptic scale. This implies, of course, that the low-level wind forecasts produced by these models are inadequate in regions where the low-level flow is strongly influenced by fine-scale topographic features. In the present study we will examine the way in which the wind field predicted by a low-resolution model can be modified so as to reflect the presence of the small scale topography following the approach suggested by Rousseau (1969). Rousseau produced a 21 hour 500 mb forecast with a barotropic primitive equation model on a hemispheric grid containing 53×57 points. The forecast height and velocity fields were then interpolated to a higher-resolution grid covering part of Europe and the integration in time was continued for a further period of three hours with a high-resolution limited-area model. In the latter model, the earth's topography was resolved in greater detail than in the hemispheric model which implied that the initial (interpolated) data on the fine mesh were out of balance. This naturally led to the propagation of gravity waves but it was found that after three hours the height and velocity fields had reached a new balance under the influence of the topography. The adjustment between the mass and velocity fields over fine-scale orography was further

¹On leave from the Atmospheric Environment Service of Canada.

examined by Rousseau (1970) using a two-dimensional baroclinic model and by Rousseau and Pham (1970) with a three-dimensional baroclinic model. In both of the latter studies the initial data supplied to the fine-mesh models were prescribed idealized conditions and adjustment periods of about two to three hours were reported. The present paper deals with similar experiments except that a fine-mesh baroclinic model is initialized from a forecast produced by a coarse-grid model. The attention will be focussed on the rate at which the flow adjusts to the new topography injected into the forecast scheme at $t = 20$ hours and on the type of circulation which is obtained after the adjustment.

The numerical model used in this study will be presented briefly in section 2. The procedure will be explained in more detail in section 3 while the results and conclusions will follow in sections 4 and 5.

2 The model and procedure

The forecasts necessary for this study were done with the primitive-equation grid-point model described by Robert, Henderson and Turnbull (1972), except that the present version of the model has a surface drag mechanism of the type discussed by Shuman and Hovermale (1968). The low-resolution horizontal grid (coarse mesh) superimposed on a polar stereographic map centered at the pole has a grid length of 381 km, true at 60°N , so that with 51×55 grid points it covers most of the Northern Hemisphere. The vertical coordinate of the model is given by $\sigma = p/p_s$, where p is the pressure and p_s is the surface pressure. The geopotential and horizontal wind components are predicted at the levels $\sigma = 0.1, 0.3, 0.5, 0.7$ and 0.9 while the "vertical velocity" $d\sigma/dt$ is carried at $\sigma = 0.2, 0.4, 0.6$ and 0.8 . The coarse-mesh model uses the terrain heights given by Berkofsky and Bertoni (1955) and the drag-coefficient field of Cressman (1960).

The area covered by the fine-mesh model is delineated by the square in Fig. 1. The locations of the coarse-mesh grid points within or on the boundary of the fine-mesh area are shown by crosses. In order to resolve topographical features such as the St. Lawrence and Richelieu Valleys, a fine-mesh grid interval of 38.1 km, one-tenth of the standard one, was adopted so that the square of Fig. 1 contained 51×51 grid points (including boundary points). The height of the terrain over the fine-mesh area was extracted from maps at every half a degree of latitude and longitude and then interpolated to the grid points. More details on the interpolation procedure can be found in Allard (1974) but it should suffice here to show the resulting contoured topographical grid-point field given in Fig. 2. It can be seen that the Laurentian Plateau (upper part of Fig. 2) and the St. Lawrence Valley (line A-B-C) are well resolved while the Richelieu Valley (B-D) creates a well defined north-south break in the Appalachians.

The values of the drag coefficient at the various grid points of the fine mesh were assigned following the method of Cressman (1960). The drag coefficient was assumed to be the sum of a first part, $C_1 = 0.13 \times 10^{-2}$, and a second part C_2 which depends on h_g , the height of the terrain above mean sea level. Using Cressman's suggested values, C_2 was assigned values which increased from 0 for

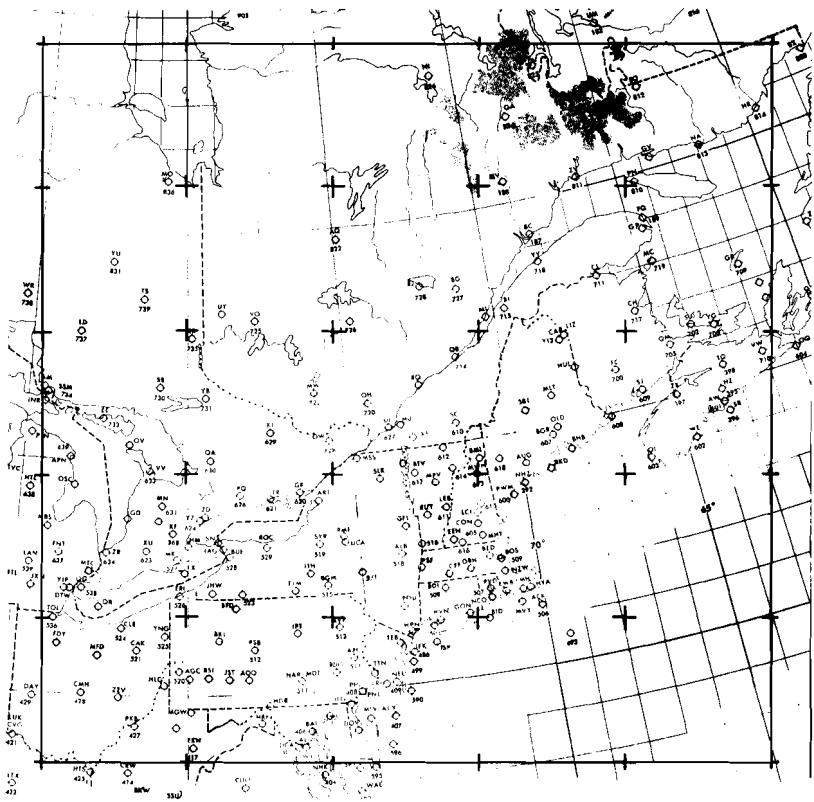


Fig. 1 The area of integration of the fine-mesh model. The grid points of the coarse-mesh model on or within the fine-mesh area are shown by crosses.

$h_p = 0$ to 0.50×10^{-2} for $h_p \geq 2750$ feet. The field of C_D , thus obtained showed values ranging from 0.13×10^{-2} to 0.63×10^{-2} over the fine-mesh area and was a mere reflection of the topography.

The procedure for the experiment was the following. Using the low-resolution topographical and drag-coefficient fields, the coarse-mesh model was integrated for 24 hours over the Northern Hemisphere, the semi-implicit formulation of the model allowing the use of one-hour time steps. The resulting 20- and 24-hour forecasts were saved, the former for further use as input to the fine-mesh model and the latter for comparison purposes. The horizontal wind and geopotential forecast fields for hour 20 were then interpolated to the fine mesh at each of the 5 sigma levels over the area shown in Fig. 1 and σ was set equal to zero. The fine-mesh limited-area model was then integrated using the high-resolution topographical and drag-coefficient fields for a further period of 4 hours (hour 20 to 24) with time steps of 6 minutes. Finally this high-resolution forecast for hour 24 was compared with the lower-resolution forecast valid for the same time.

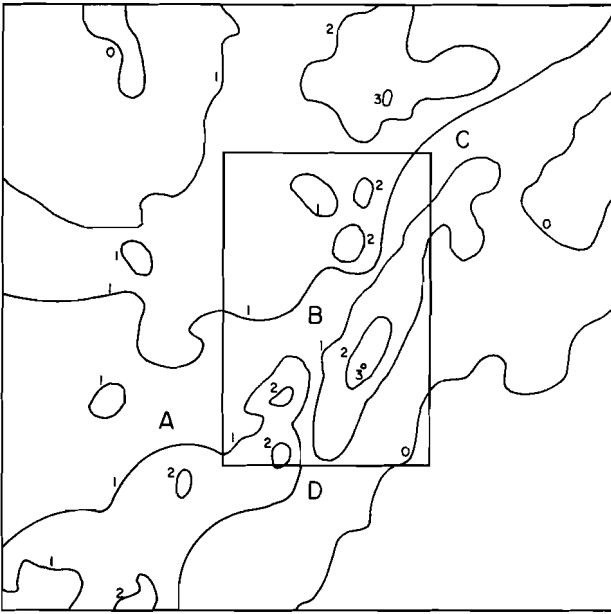


Fig. 2 Fine-mesh topographical field in thousands of feet.

For the fine-mesh forecast both horizontal wind components and the normal gradient of the surface pressure were kept fixed in time along the outer boundary of Fig. 2. Such simplified boundary conditions are of course applicable only for very short forecasts and there is little doubt that the use of time-dependent boundary conditions would constitute an improvement. It was felt, however, that in a first approach with the present model it would be justifiable to test the general procedure with time-independent boundary conditions especially since the fine-mesh integration extends only over 4 hours, over which time period the flow at the boundary can change very little. Further, in order to minimize the effect of the boundary conditions on the results to be discussed in the subsequent sections, only that part of the forecast within the inner rectangle of Fig. 2 was retained for discussion. It should be noted that the latter area is sufficiently large to include the Richelieu Valley and the major portion of the St. Lawrence Valley.

The above procedure implies that for the first 20 hours the small-scale to large-scale interactions are neglected, except for the fact that the drag coefficient used in the large-scale model increases in mountainous areas to simulate the drain of energy on the large scale by mountain-generated gravity waves (Cressman, 1960). While the approach will be assumed valid for the present study, where the small-scale orographic features have relatively small amplitudes, it should be realized that a more sophisticated approach may be required in areas of very large amplitude small-scale topography.

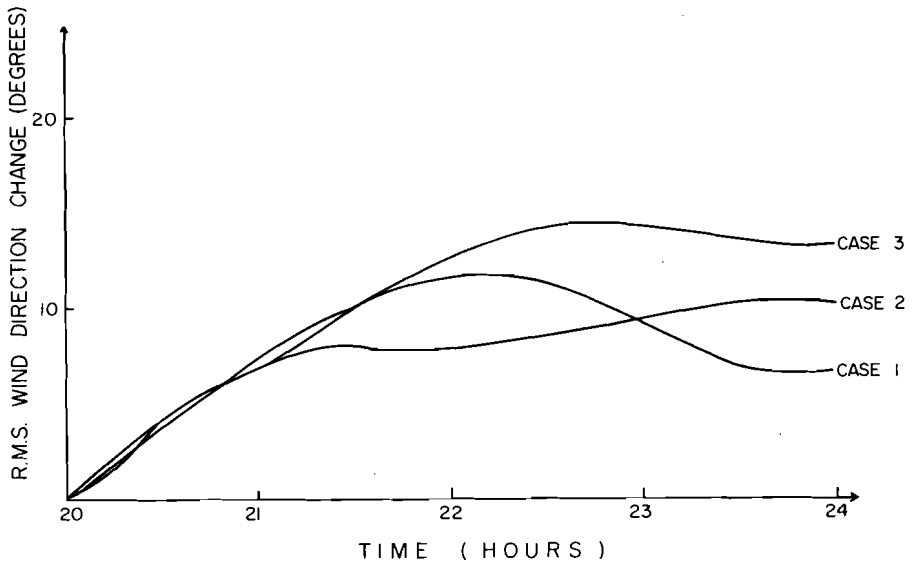


Fig. 3 Root mean square of the wind direction change (relative to $t = 20$ hours), in degrees, as a function of time for the fine-mesh model.

3 The time evolution of the fine-mesh forecasts

An inspection of the fine-mesh wind-direction field displayed at regular intervals of 30 minutes (5 time steps) at $\sigma = 0.9$ (not shown here) indicated that the latter varied continuously for the first 3 hours or so, after which definite patterns were established. To represent this time evolution quantitatively, the root mean square of the difference between the wind direction at time t and that at $t = 20$ hours was computed at the level $\sigma = 0.9$. The results are presented in Fig. 3 for three different sets of initial data: CASE 1 (00Z, 26 March 1971), CASE 2 (00Z, 13 January 1973) and CASE 3 (00Z, 7 April 1973). The time evolution mentioned earlier is clearly shown for cases 2 and 3 and, to a lesser extent for case 1. We note, in particular, that after about 4 hours the high-resolution topographical influence on the wind direction is of the order of 10 degrees.

The introduction of the high-resolution topographical and drag-coefficient fields at $t = 20$ hours can clearly be expected to lead to the generation of gravity waves. During the integration the high frequency part of the wave spectrum has been damped with time by the use of a frequency filter incorporated into the finite-difference time-stepping scheme. The latter has the form

$$F^*(t+\Delta t) = F(t-\Delta t) + 2\Delta t(\partial F/\partial t)^*,$$

$$F(t) = F^*(t) + 0.5\nu [F^*(t+\Delta t) - 2F^*(t) + F(t-\Delta t)],$$

which was first used by Robert (1966). In the above, an asterisk represents a preliminary value and the absence of an asterisk indicates the final value. For

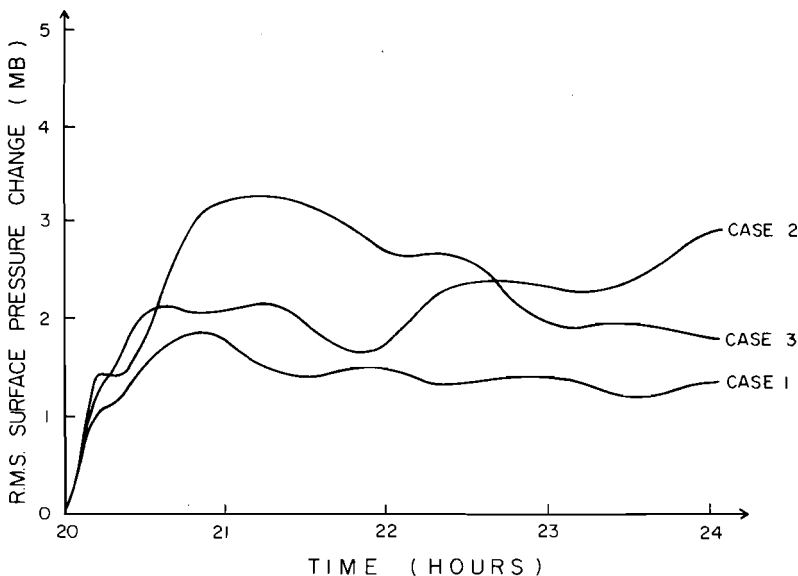


Fig. 4 Root mean square of the surface pressure change (relative to $t = 20$ hours), in mb, as a function of time for the fine-mesh model.

the fine-mesh model ν was set equal to 0.33. The characteristics of the filter have been discussed by Asselin (1972).

The root mean square surface pressure change (relative to $t = 20$ hours) was also computed as a function of time in the fine-mesh model. The results, shown in Fig. 4, indicate that an important fraction of the adjustment in the surface pressure takes place within the first hour of the fine-mesh integration. This stands in contrast with the wind direction field at $\sigma = 0.9$ (Fig. 3) which adjusts more gradually to the new topography and surface friction. In other words, the vertically integrated mass field changes appear to result mainly from relatively fast wave motions while the low-level wind-direction field adjustment seems to reflect the presence of slower oscillations, most likely of the internal gravity-wave type.

As already mentioned, Rousseau and Pham (1970) have obtained adjustment periods of about two to three hours in similar experiments. Their fine-grid primitive-equation baroclinic model was initialized by means of an idealized flow in geostrophic balance and integrated with a centered time scheme without frequency filter, using cyclic boundary conditions in the horizontal. Considering the present results shown in Figs. 3 and 4 and the fact that Rousseau and Pham seem to have estimated the adjustment period by a qualitative inspection of the predicted fields, it would appear that the two independent estimates of the adjustment period are not significantly different.

In the next section some fine-mesh forecast fields at $t = 24$ hours will be discussed and comparisons will be made with the coarse-mesh forecast valid at the same time.

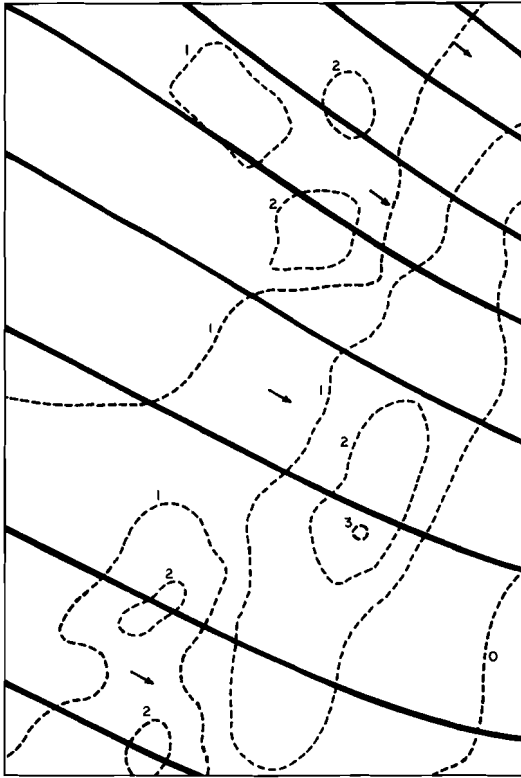


Fig. 5 Streamlines (solid lines) at $\sigma = 0.9$ resulting from a 24-hour coarse-grid integration. The dashed lines are topographical contours at every thousand feet (used in fine-mesh model only). They will appear on all subsequent figures.

4 The wind forecast after the adjustment period

We will now examine some of the forecast fields for CASE 1 (CASES 2 and 3 yielded similar results). Fig. 5 shows the streamlines at $\sigma = 0.9$ over the inner rectangle of Fig. 2, as obtained from the 24-hour coarse-grid integration. The dashed lines are the contours of the high-resolution topography. They are presented here for reference only, since they were not used in the coarse-grid integration. It should be noticed that the case being examined is one in which the predicted low-level wind is from the northwest.

After subtracting the coarse-grid wind-direction field from the fine-mesh one valid at the same time, the difference field shown in Fig. 6 was obtained. It can be seen that the fine-mesh low-level wind rotated clockwise by up to 24 degrees in the Richelieu Valley thus becoming more nearly parallel to the north-south valley. On the other hand, a counter-clockwise rotation of up to 18 degrees was obtained near the centre of the figure, showing the channelling effect of the valley between the higher ground to the north and south.

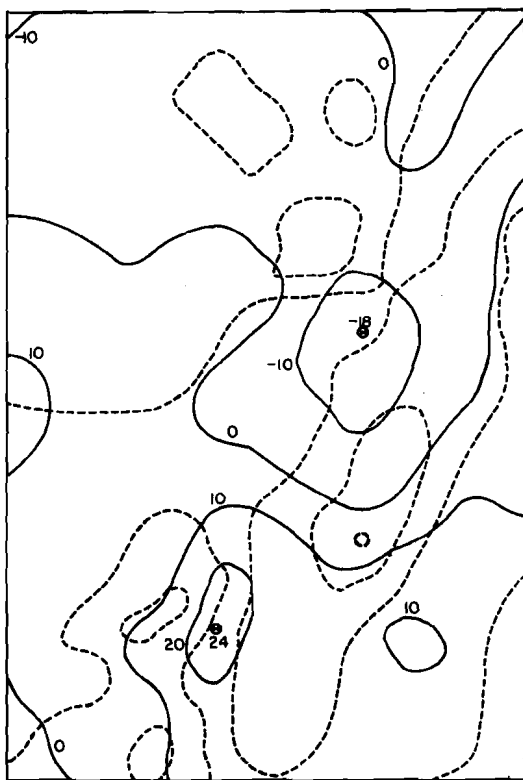


Fig. 6 Difference in wind direction (degrees) between fine- and coarse-grid forecasts at $\sigma = 0.9$, $t = 24$ hours. A positive (negative) value means that the fine-mesh wind was rotated clockwise (counterclockwise) with respect to the coarse-mesh wind.

The isotachs at $\sigma = 0.9$ resulting from the 24-hour coarse-grid integration are presented in Fig. 7 while the difference between the coarse-grid and fine-grid wind speeds is shown in Fig. 8. It can be seen that in general the fine-mesh model yields lower wind speeds over the St. Lawrence Valley and higher wind speeds over the higher terrain, as compared to the coarse-mesh model. In other words, the air is found to accelerate as it flows over an obstacle and to decelerate as it comes to a valley.

The horizontal wind divergence field at $\sigma = 0.9$ resulting from the fine-mesh integration is presented in Fig. 9. While there is relatively little divergence or convergence over nearly uniform terrain, areas of large divergence and convergence are found on the windward side and lee side, respectively, of the higher mountains. This is in agreement with the earlier results which showed, in particular, that on the windward side of a mountain part of the flow accelerated in going over the mountain while the rest of the flow was deflected around it.

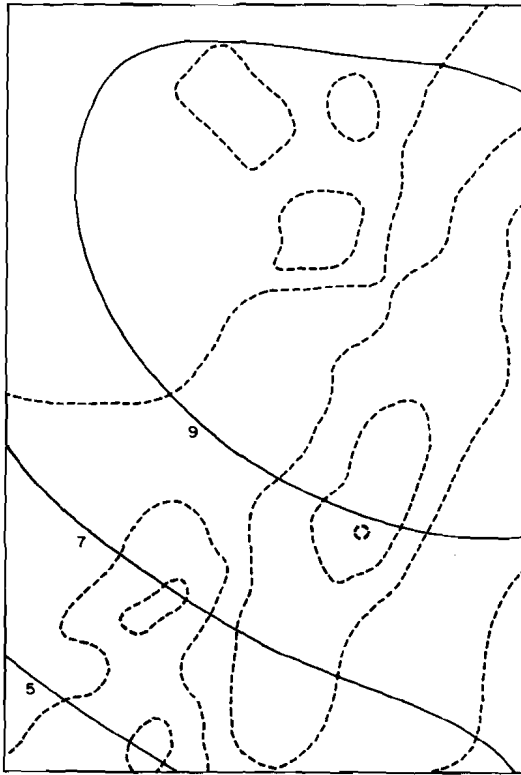


Fig. 7 Isotachs (m s^{-1}) at $\sigma = 0.9$ resulting from a 24-hour coarse-grid integration.

The vertical velocity $\omega = dp/dt$ at $\sigma = 0.9$ is shown in Fig. 10 in units of $\mu\text{b s}^{-1}$. Remembering that the flow is generally from the northwest it is not surprising to find the regions of negative ω (rising motion) on the windward side of the mountainous areas and the areas of positive ω (sinking motion) on the leeward side. Maximum values of $\pm 5 \mu\text{b s}^{-1}$ (about $\pm 5 \text{ cm s}^{-1}$) as well as maximum gradients are found near the roughest areas. Over the Atlantic (southeast corner) and the Laurentian Plateau (northwest region) the vertical motion remains very small while the air is slowly sinking on the northern side of the St. Lawrence Valley and rising on its southern side.

5 Conclusion

The numerical experiments indicated that a period of about three to four hours is required for a large-scale flow-pattern to adjust reasonably well to the fine-scale topography. The deflecting action of the main mountains and valleys was demonstrated and the vertical-motion field created by the air flow over the topography was discussed.

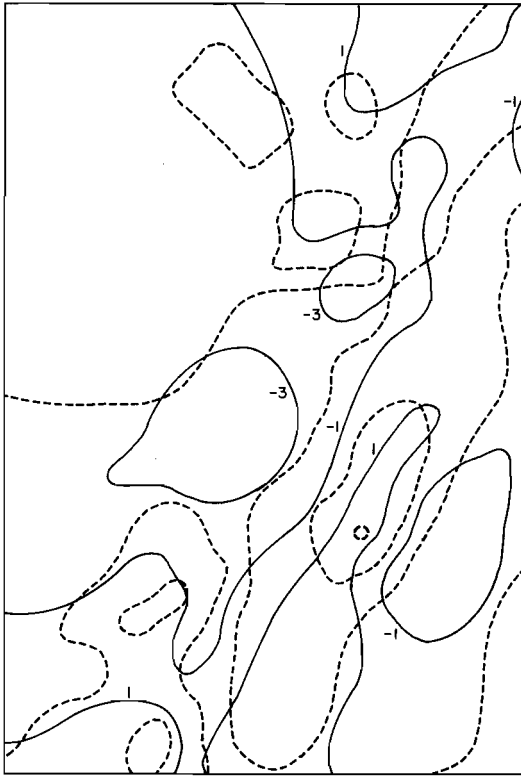


Fig. 8 Difference in wind speed at $\sigma = 0.9$, $t = 24$ hours, between fine- and coarse-grid forecasts, in m s^{-1} . A positive (negative) value means a greater (smaller) wind speed in the fine-mesh forecast.

It appears that with suitable refinements the procedure used in this study could be of practical value for regional forecasting. The present model would require approximately 20 minutes of computer time on the CDC Cyber 76 to produce a 36-hour adjusted forecast (about 10 minutes for the initialization and 32-hour coarse-grid hemispheric forecast and about 10 minutes for the 4-hour limited-area fine-mesh forecast).

One of the refinements which should be included in the model in further experiments has already been mentioned, namely, the use of time-dependent boundary conditions. A further improvement in the results could also be expected by increasing the number of "horizontal" levels of the models since the short scale features discussed in this paper are rather shallow (only minor effects on the wind field were obtained at $\sigma = 0.7$ while the flow was essentially undisturbed at $\sigma = 0.5$ by the small-scale topography). Finally the usefulness of the approach would be enhanced by the introduction of the moisture equation in the model since the latter could then produce quantitative forecasts of orographic clouds and precipitation rates.

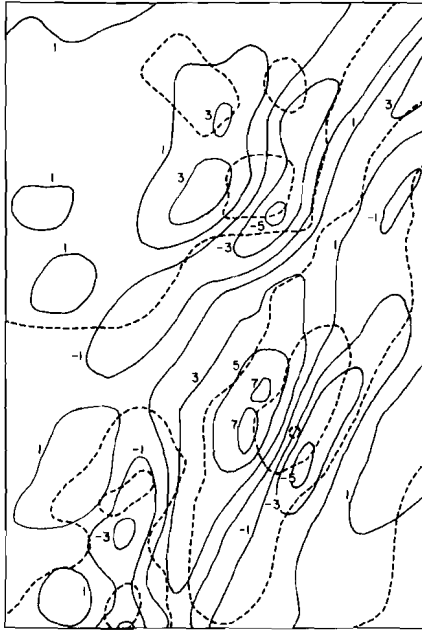


Fig. 9 The horizontal wind divergence field of the fine-mesh forecast at $\sigma = 0.9$, $t = 24$ hours, in units of 10^{-5} s^{-1} .

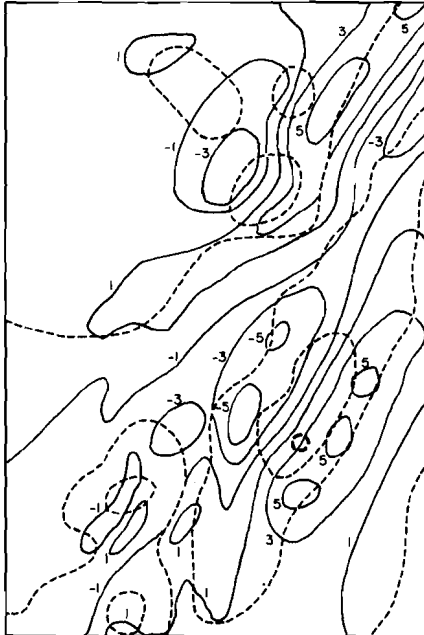


Fig. 10 The vertical motion ω for the fine-mesh forecast at $\sigma = 0.9$, $t = 24$ hours in $\mu\text{b s}^{-1}$.

Acknowledgements

The cooperation of the staff of the Dynamic Prediction Research Division of the Atmospheric Environment Service is noted with appreciation. They not only supplied the model used in the experiments but also provided guidance on the introduction of some modifications to the computer program. The second author also wishes to acknowledge the financial support received through a grant from the National Research Council of Canada.

References

- ALLARD, H., 1974: Adjustment of regional wind forecasts to the topography. M.Sc. Thesis, Dept. of Meteorology, McGill University, 87 pp.
- ASSELIN, R., 1972: Frequency filter for time integrations. *Mon. Wea. Rev.*, **100**, 487-490.
- BERKOFSKY, L., and E.A. BERTONI, 1955: Mean topographic charts for the entire earth. *Bull. Amer. Meteor. Soc.*, **36**, 350-354.
- CRESSMAN, G.P., 1960: Improved terrain effects in barotropic forecasts. *Mon. Wea. Rev.*, **88**, 327-342.
- ROBERT, A.J., 1966: The integration of a low order spectral form of the primitive meteorological equations. *J. Meteor. Soc. Japan*, **44**, 237-245.
- , J. HENDERSON and C. TURNBULL, 1972: An implicit time integration scheme for baroclinic models of the atmosphere. *Mon. Wea. Rev.*, **100**, 329-335.
- ROUSSEAU, D., 1969: Expérience préliminaire à l'élaboration d'un modèle numérique de prévision régionale. *La Météorologie*, Série 5, No. 9, 5-23.
- , 1970: Etude numérique de l'action du relief sur l'atmosphère. Modèle bidimensionnel. *La Météorologie*. Série 5, No. 14, 1-23.
- , and H.L. PHAM, 1970: Etude numérique de l'action du relief sur l'atmosphère. Modèle tridimensionnel. *La Météorologie*, Série 5, No. 14, 25-41.
- SHUMAN, F.G. and J.B. HOVERMALE, 1968: An operational six-layer primitive equation model. *J. Appl. Meteor.*, **7**, 525-547.